

Rare B decays at LHCb

T. Blake^{1,a} on behalf of the LHCb collaboration

¹CERN, Switzerland

Abstract. Rare B meson decays are an ideal place to search for the effects of new particles that could arise in extensions to the Standard Model and couple to the flavour sector. Measurements of the rare B decay processes at LHCb are presented. The relationship between these different measurements is described. Finally, the implication of these measurements for SUSY/Exotic searches is discussed.

1 Introduction

The phrase “rare decay” is often used to describe a set of flavour changing neutral current processes that, are forbidden at tree level, and are mediated by electroweak box and penguin type diagrams in the Standard Model. These processes include: radiative $b \rightarrow s\gamma$ transitions; decays of B mesons to a pair of opposite charge leptons and semileptonic $b \rightarrow s\ell^+\ell^-$ (where $\ell = e, \mu, \tau$) decays. In many extensions to the SM, these rare decay processes can receive contributions from new virtual particles that can enhance (or suppress) the branching fraction of the decays or change the angular distribution of the B decay products.

2 Effective field theory for $b \rightarrow s$ processes

The phenomenology of rare B meson decays is a multi-scale problem; at one end, the electroweak-scale of the weak interaction and at the other end, Λ_{QCD} . Rare $b \rightarrow s$ decay processes can therefore be treated using an effective field theory, with a Hamiltonian

$$\mathcal{H}_{\text{eff}} = -\frac{4G_F}{\sqrt{2}} V_{tb} V_{ts}^* \sum_{\text{SM}} C_{\text{SM}} O_{\text{SM}} + \sum_{\text{NP}} C_{\text{NP}} O_{\text{NP}}, \quad (1)$$

where G_F is the Fermi constant and the $V_{tb} V_{ts}^*$ the product of CKM matrix elements. The O are local operators with different Lorentz structures and the C are Wilson coefficients that contain information on the heavy degrees of freedom (the top-quark, W^\pm , Z^0 and Higgs in the SM). Finally, in extensions to the SM it is possible to have new particles, at a mass scale Λ_{NP} , that contribute to the SM set of local operators or introduce entirely new operators with $C_{\text{NP}} \propto 1/\Lambda_{\text{NP}}$.

Different processes receive contributions from different local operators. Radiative decays of B mesons, which at the quark level correspond to a $b \rightarrow s\gamma$ transition, for

^ae-mail: thomas.blake@cern.ch

example are governed by the magnetic penguin operator that is commonly labelled O_7 . The purely leptonic decay $B_s^0 \rightarrow \mu^+\mu^-$ is governed by the axial-vector operator (O_{10}) and semileptonic $b \rightarrow s\ell^+\ell^-$ decays receive contributions from O_7 , O_{10} and the vector operator O_9 .

In the SM, contributions to the right-handed counterparts of O_7 , O_9 and O_{10} , labelled below with a prime, are highly suppressed (by m_s/m_b) as are contributions to scalar, O_S , or pseudoscalar, O_P , operators. Contributions to these operators can be significantly enhanced in many extensions to the SM.

3 Radiative decays

There is a wealth of information on C_7 and C_7' from measurements of radiative $b \rightarrow s\gamma$ decays at the B-Factories and CLEO-c, see for example Ref. [1]. The two most stringent constraints come from measurements of the inclusive branching fraction, $\mathcal{B}(b \rightarrow s\gamma)$, which constrains $|C_7|^2 + |C_7'|^2$ but does not distinguish between C_7 and C_7' , and measurements of time dependent CP violation in $B^0 \rightarrow K^{*0}\gamma$ ($K^{*0} \rightarrow K^0\pi^0$) decays, $S_{K^{*0}\gamma}$, which constrains C_7/C_7' . These constraints on C_7 and C_7' are shown in Fig. 5. Unfortunately both measurements are challenging in a hadronic environment and are unlikely to be improved by LHCb.

At LHCb however, additional constraints on C_7 and C_7' can be determined: from the lifetime dependence of $B_s^0 \rightarrow \phi\gamma$ decays [2]; from measurements of the photon and proton angular distributions in radiative Λ_b decays [3, 4] and from asymmetries in B decays to final states containing a photon, a pseudoscalar and a vector meson such as $B^+ \rightarrow \phi K^+\gamma$ [5, 6].

To highlight the potential of the radiative decay programme of LHCb, the $K^+\pi^-\gamma$ and $K^+K^-\gamma$ invariant mass of $B^0 \rightarrow K^{*0}\gamma$ and $B_s^0 \rightarrow \phi\gamma$ candidates, in a data sample of 1 fb^{-1} , are shown in Fig. 1. Signals of 5279 ± 93 and 601 ± 36 candidates are seen for $B^0 \rightarrow K^{*0}\gamma$ and $B_s^0 \rightarrow \phi\gamma$ respectively [7]. These samples are far larger than the sam-

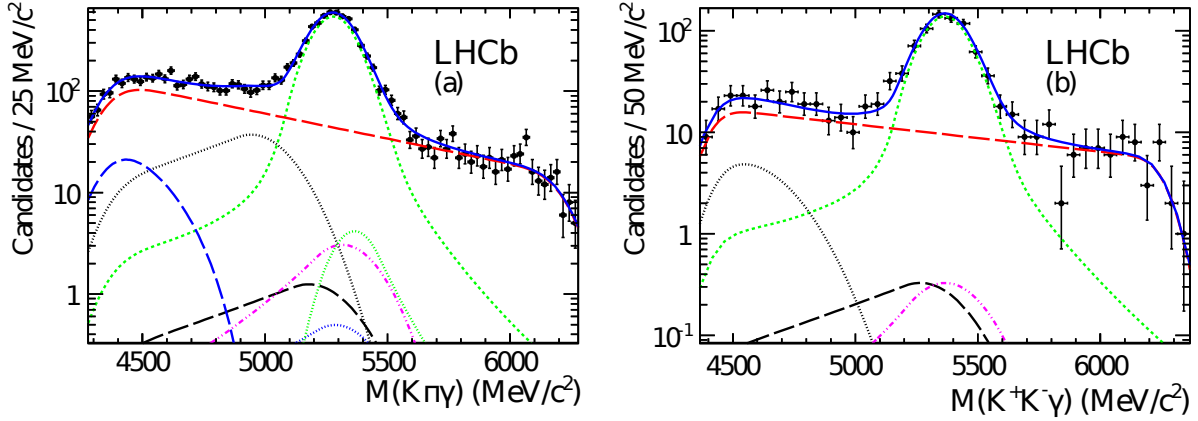


Figure 1. $K^+\pi^-\gamma$ (left) and $K^+K^-\gamma$ (right) invariant mass of selected $B^0 \rightarrow K^{*0}\gamma$ and $B_s^0 \rightarrow \phi\gamma$ candidates. The fit components are: the signal (green dotted); combinatorial background (red dashed); $\Lambda_b \rightarrow p^+K^-\gamma$ (purple dot-dashed); $B^+ \rightarrow K^+\pi^-\pi^0$ and $B_s^0 \rightarrow K^+K^-\pi^0$ (black long-dashed and blue dotted); partially reconstructed decays with one or more missing particles (blue dashed and black dotted).

ples available at the B-factories and importantly show that the various sources of background can be controlled.

4 Leptonic decays

The branching fraction of the decays $B_s^0 \rightarrow \mu^+\mu^-$ and $B^0 \rightarrow \mu^+\mu^-$ are suppressed both by the loop-order of the process and by helicity in the SM. In the SM, the branching fractions scale as $C_{10} - C'_{10}$. In extensions to the SM, in which there are large contributions to either scalar or pseudo-scalar operators (denoted C_S and C_P), the branching fraction of the decay can see large enhancements,

$$\mathcal{B}(B_s^0 \rightarrow \mu^+\mu^-) \propto \left(1 - \frac{4m_\mu^2}{m_B^2}\right) |C_S - C'_S|^2 + |C_P - C'_P + \frac{2m_\mu^2}{M_B^2}(C_{10} - C'_{10})|^2. \quad (2)$$

Large contributions to C_S and C_P often arise in models with extended Higgs sectors, e.g. in SUSY models or models with two Higgs-doublets.

In LHCb, $B_s^0 \rightarrow \mu^+\mu^-$ candidates are selected using a loose pre-selection and are then classified using a BDT based on the kinematic properties of the reconstructed B_s^0 candidate. The analysis procedure is described in detail in Ref. [8]. The dimuon invariant mass of the candidates with a signal-like BDT response is shown in Fig. 2. LHCb observes a signal that is incompatible with the background only hypothesis at 3.5σ , providing the first evidence for the $B_s^0 \rightarrow \mu^+\mu^-$ decay.

Normalising the observed yield with respect to $B^+ \rightarrow J/\psi K^+$ and $B^0 \rightarrow K^+\pi^-$ and accounting for the ratio of fragmentation fractions, f_s/f_d , yields

$$\mathcal{B}(B_s^0 \rightarrow \mu^+\mu^-) = (3.2^{+1.5}_{-1.2}) \times 10^{-9}.$$

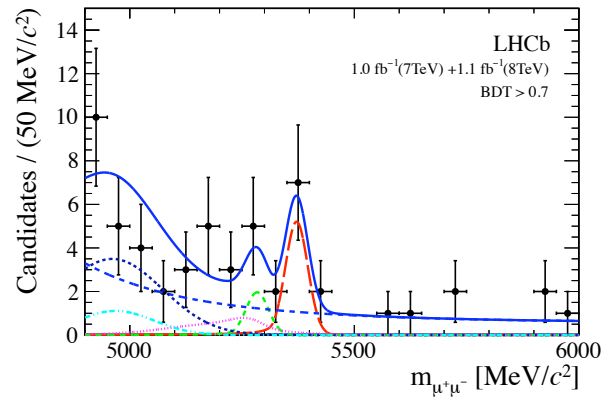


Figure 2. Dimuon invariant mass of $B_s^0 \rightarrow \mu^+\mu^-$ candidates with signal-like BDT responses. The fit components are: the $B_s^0 \rightarrow \mu^+\mu^-$ signal (red long-dashed); $B^0 \rightarrow \mu^+\mu^-$ (green medium-dashed); $B^0 \rightarrow K^+\pi^-$, $B^0 \rightarrow \pi^+\pi^-$ and other $B_{(s)} \rightarrow h^+h^-$ peaking backgrounds (pink dotted); $B^0 \rightarrow \pi^-\mu^+\gamma_\mu$ (black short-dashed); $B \rightarrow \pi\mu^+\mu^-$ (light blue dot-dashed); combinatorial background (blue medium dashed).

This should be compared to a time-integrated SM expectation [9, 10] of

$$\mathcal{B}(B_s^0 \rightarrow \mu^+\mu^-) = (3.5 \pm 0.3) \times 10^{-9},$$

which is clearly in good agreement with the observed limit. Barring fortuitous cancellation (e.g. $C_S = C'_S$ or $C_P = C'_P$) this rules out large contributions from either C_S or C_P to the branching fraction.

5 Semileptonic decays

The most stringent experimental constraints on axial-vector and vector operators come from semileptonic B meson decays, in particular from the branching fraction and

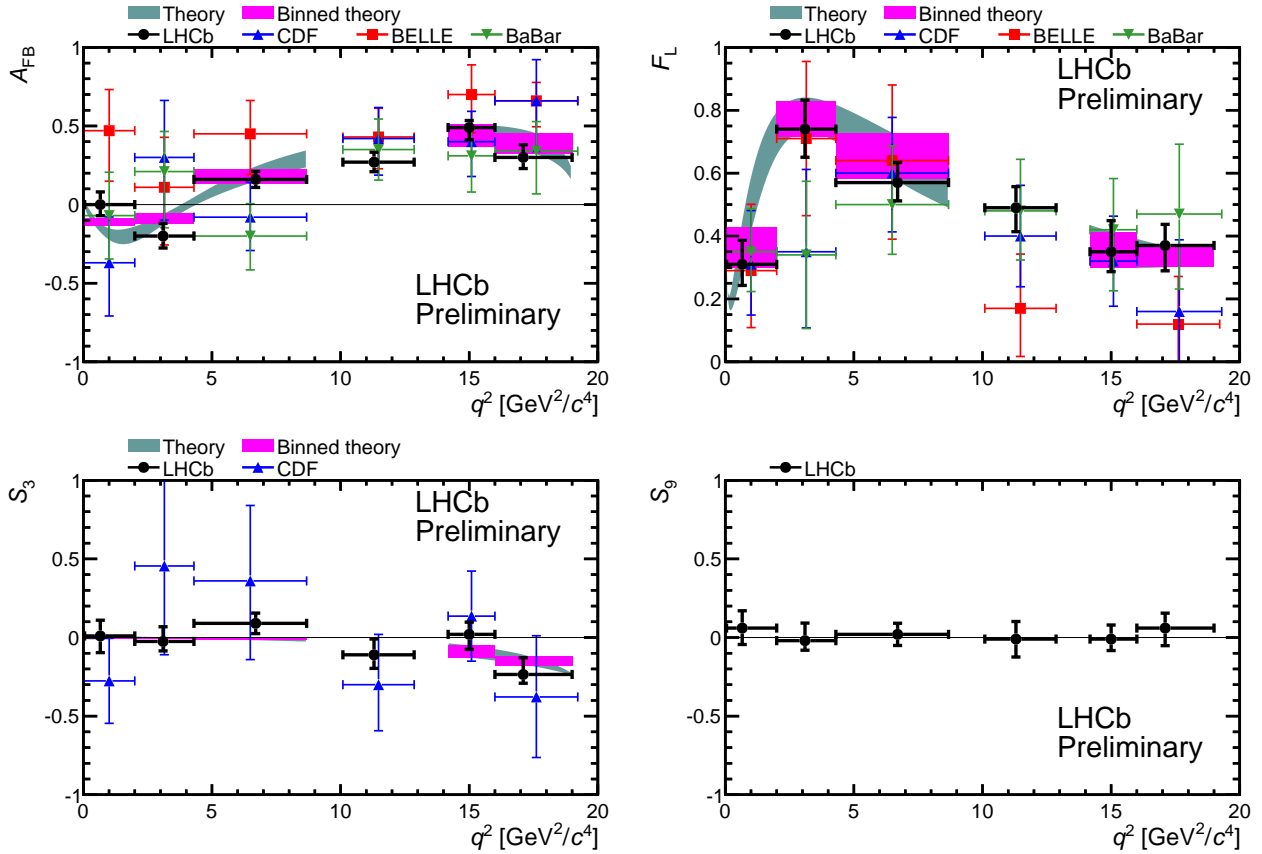


Figure 3. Angular observables in the $B^0 \rightarrow K^{*0} \mu^+ \mu^-$ decay: dimuon system forward backward asymmetry, A_{FB} (top left); fraction of longitudinal polarisation of the K^{*0} , F_L (top right), a term proportional to the asymmetry between the two transverse amplitudes (S_3). The observable S_9 is suppressed by small strong phases and is a null-test.

angular distribution of $B^0 \rightarrow K^{*0} \mu^+ \mu^-$ and $B^+ \rightarrow K^+ \mu^+ \mu^-$ decays.

5.1 The $B^0 \rightarrow K^{*0} \mu^+ \mu^-$ decay

The four-body final state of the $B^0 \rightarrow K^{*0} \mu^+ \mu^-$ decay can be described in terms of three angles (θ_ℓ , θ_K and ϕ) and the invariant mass squared, q^2 , of the dimuon system (see for example Ref. [11])

$$\frac{d^4\Gamma}{dq^2 d\cos\theta_\ell d\cos\theta_K d\phi} = \sum_{i=0}^9 J_i(q^2) f_i(\cos\theta_\ell, \cos\theta_K, \phi). \quad (3)$$

The J_i are bilinear combinations of K^{*0} spin-amplitudes that in turn depend on the Wilson coefficients $C_7^{(\prime)}$, $C_9^{(\prime)}$ and $C_{10}^{(\prime)}$ and $B \rightarrow K^{*0}$ form-factors (the contribution from C_S and C_P to the angular distribution is small). The dominant theoretical uncertainties arise from the form-factors and can be mitigated by forming angular observables in which the form-factor uncertainties can be cancelled.

Due to the limited size of the available data samples (900 candidates in LHCb), the angular distribution is simplified by transforming the ϕ angle or integrating over two of the three angles. This leaves four free parameters: the fraction of longitudinal polarisation of the K^{*0} , F_L ; the

forward backward asymmetry of the dimuon system, A_{FB} ; and a parameter that is sensitive to the asymmetry between the transverse K^{*0} spin amplitudes, S_3 . In the preliminary LHCb result, the fourth parameter, S_9 , is suppressed by small strong phases and is expected to be close to zero.

Figure 3 shows the values of A_{FB} , F_L , S_3 and S_9 measured by the LHCb [12], BaBar [13], Belle [14] and CDF [15] experiments in six bins of q^2 . The results are consistent between the different experiments and consistent with the SM expectation (which is included in the figure).

In the SM A_{FB} varies with q^2 and changes sign at $q_0^2 \sim 4 \text{ GeV}^2/c^4$ due to the interplay between C_7 and C_9 . This behaviour is reproduced by the LHCb data. Fitting forward- and backward-going events separately as a function of q^2 gives a zero crossing point,

$$q_0^2 = 4.9_{-1.1}^{+1.3} \text{ GeV}^2/c^4.$$

The presence of this crossing point fixes the sign of C_7 with respect to C_9 .

5.2 The $B^+ \rightarrow K^+ \mu^+ \mu^-$ decay

The $B^+ \rightarrow K^+ \mu^+ \mu^-$ decay can be described by a single angle, θ_ℓ , defined in the rest frame of the dimuon system [16]

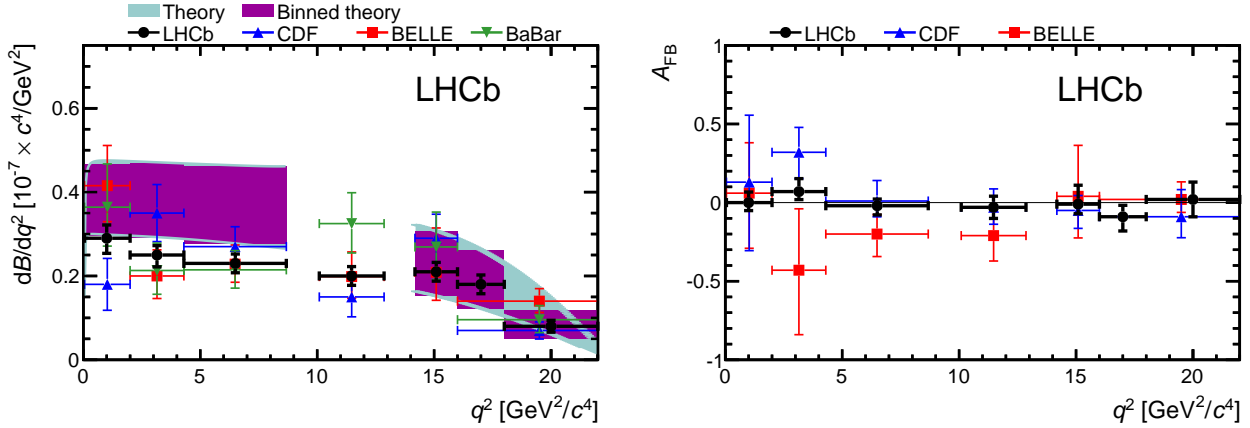


Figure 4. Differential branching fraction (left) and dimuon system forward backward asymmetry (right) of the $B^+ \rightarrow K^+ \mu^+ \mu^-$ decay. The forward-backward asymmetry of the decay is expected to be zero in the SM.

$$\frac{1}{\Gamma} \frac{d\Gamma[B^+ \rightarrow K^+ \mu^+ \mu^-]}{d\cos\theta_\ell} = \frac{3}{4}(1 - F_H)(1 - \cos^2\theta_\ell) + \frac{1}{2}F_H + A_{FB} \cos\theta_\ell, \quad (4)$$

and two parameters, the forward backward asymmetry of the dimuon system, A_{FB} and a parameter F_H . In the SM A_{FB} is vanishingly small and F_H tends to be close to zero. Both A_{FB} and F_H can be significantly enhanced in models in which $C_S^{(\prime)}$ or $C_P^{(\prime)}$ are large or in models which give rise to new local operators that have a tensor-like Lorentz structure (which can occur in Leptoquark models) [17].

In contrast to the decay $B_s^0 \rightarrow \mu^+ \mu^-$ the (differential) branching fraction of the decay scales as

$$\frac{d\mathcal{B}}{dq^2} \propto |(C_{10} + C'_{10})f_+(q^2)|^2 + |(C_9 + C'_9)f_+(q^2) + \frac{2m_b}{M_B + M_K}(C_7 + C'_7)f_T(q^2)|^2. \quad (5)$$

Measurements of A_{FB} , F_H and $d\mathcal{B}/dq^2$ at LHCb are described in Ref. [18]. Using 1 fb^{-1} of integrated luminosity, LHCb observes 1232 ± 40 candidates with an excellent signal-to-background ratio.

Figure 4 shows the differential branching fraction and of A_{FB} measured by the LHCb [18], BaBar [13], Belle [14] and CDF [15] experiments in six bins of q^2 . These are largely compatible with the SM expectation but favour a smaller branching fraction at low q^2 than is predicted in the SM. The parameter F_H is not shown but is also compatible with the SM.

6 Implications of recent measurements

A global combination of the various rare decay measurements has been made by several groups. An example from Ref. [20] is shown in Fig. 5. By combining several

measurements, more stringent constraints are achieved on non-SM contributions to the Wilson coefficients. Unfortunately, the individual measurements and the global combination is in good agreement with the SM (which corresponds to $C'_{(7,9,10)} = 0$ and $C_{7,9,10}^{\text{NP}} = 0$).

Translating these constraints on the Wilson coefficients into constraints on the masses of new particles in extensions to the SM is highly model dependent. In models that would introduce tree-level FCNC's, the constraints on the Wilson coefficients typically imply the mass scale of the new particles, Λ_{NP} , is $\mathcal{O}(10 - 100 \text{ TeV})$. In many SUSY/Exotic scenarios, the new particle contributions are loop-suppressed and typically enter with the same CKM-like hierarchy as the SM. In such scenarios, the constraints from rare decay measurements are weakened but still imply Λ_{NP} is in the range $100 \text{ GeV} - 1 \text{ TeV}$.

Studies have also been carried out in specific models. In the CMSSM for example (Ref. [19]), the branching fraction of the $B_s^0 \rightarrow \mu^+ \mu^-$ decay scales approximately as $\tan^6\beta/M_A^4$. At $\tan\beta = 50$, the $B_s^0 \rightarrow \mu^+ \mu^-$ branching fraction measurement excludes regions of the $m_0 : m_{1/2}$ plane with masses below 1 TeV . At these large values of $\tan\beta$ the indirect constraints from rare decay measurements can be stronger than the limits from direct searches at ATLAS and CMS (see Fig. 6).

7 Conclusion

The rare decay programme of LHCb is a very active area. New results will appear in the near future from the full 2011 and 2012 data sets and 3 fb^{-1} of integrated luminosity. This larger data set will enable LHCb to improve its existing measurements and will open up new avenues of exploration in rare $b \rightarrow s$ and rare $b \rightarrow d$ processes (that have not been discussed in these proceedings).

References

- [1] S. Descotes-Genon, D. Ghosh, J. Matias, M. Ramon, JHEP **06**, 099 (2011), 1104.3342

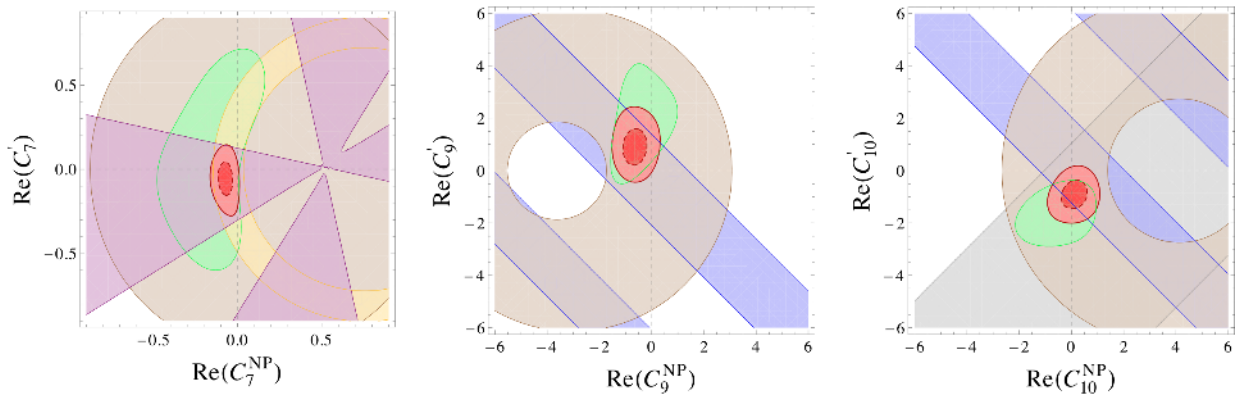


Figure 5. Constraints on $C_7^{(f)}$ (left) from measurements of $\mathcal{B}(b \rightarrow s\gamma)$ (yellow doughnut), $\mathcal{B}(b \rightarrow s\ell^+\ell^-)$, where $\ell = \mu, e$ (large brown circle), $S_{K^*\gamma}$ (purple cross) and the angular analysis of $B^0 \rightarrow K^{*0}\mu^+\mu^-$ (complex green region). Constraints on $C_9^{(f)}$ and $C_{10}^{(f)}$ (center and right) from measurements of $\mathcal{B}(b \rightarrow s\ell^+\ell^-)$ (brown doughnut), $\mathcal{B}(B^+ \rightarrow K^+\mu^+\mu^-)$ (twin blue bands), $\mathcal{B}(B_s^0 \rightarrow \mu^+\mu^-)$ (wide grey band in $C_{10}^{(f)}$ plane) and the angular analysis of $B^0 \rightarrow K^{*0}\mu^+\mu^-$ (complex green region). The constraints are given at the 90% CL. The combined constraint is also shown (in red). The SM point corresponds to the intercept of the dashed lines. Figure reproduced from Ref. [20].

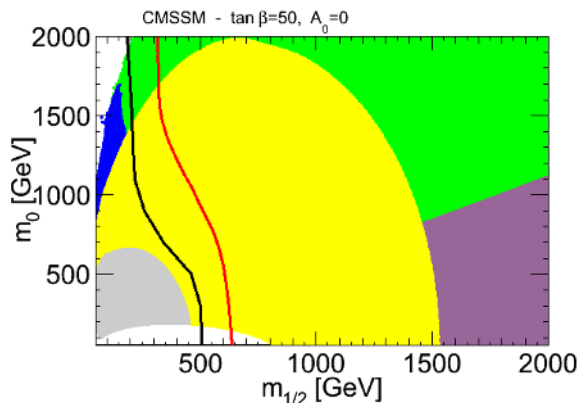


Figure 6. Constraints in the $m_0 : m_{\frac{1}{2}}$ plane of the CMSSM at $\tan\beta = 50$ from the branching fraction of $B_s^0 \rightarrow \mu^+\mu^-$ (yellow region) and direct searches (red and black lines) at CMS with up to 5 fb^{-1} of integrated luminosity. The allowed region is also indicated (in green). Figure reproduced from Ref. [19].

- [2] F. Muheim, Y. Xie, R. Zwicky, Phys.Lett. **B664**, 174 (2008), 0802.0876
- [3] F. Legger, T. Schietinger (2006), CERN-LHCB-2006-013
- [4] G. Hiller, M. Knecht, F. Legger, T. Schietinger, Phys.Lett. **B649**, 152 (2007), hep-ph/0702191
- [5] M. Gronau, D. Pirjol, Phys.Rev. **D66**, 054008 (2002), hep-ph/0205065

- [6] D. Atwood, T. Gershon, M. Hazumi, A. Soni (2007), hep-ph/0701021
- [7] R. Aaij et al. (LHCb Collaboration), Nucl.Phys. **B867**, 1 (2013), 1209.0313
- [8] R. Aaij et al. (LHCb Collaboration) (2012), 1211.2674
- [9] A.J. Buras, J. Girrbach, D. Guadagnoli, G. Isidori, Eur.Phys.J. **C72**, 2172 (2012), 1208.0934
- [10] K. De Bruyn, R. Fleischer, R. Knegjens, P. Koppenburg, M. Merk et al., Phys.Rev. **D86**, 014027 (2012), 1204.1735
- [11] W. Altmannshofer, P. Ball, A. Bharucha, A.J. Buras, D.M. Straub et al., JHEP **01**, 019 (2009), 0811.1214
- [12] LHCb collaboration (2012), LHCb-CONF-2012-008
- [13] J.P. Lees et al. (BaBar collaboration), Phys.Rev. **D86**, 032012 (2012), 1204.3933
- [14] J.T. Wei et al. (Belle collaboration), Phys.Rev.Lett. **103**, 171801 (2009), 0904.0770
- [15] T. Aaltonen et al. (CDF collaboration), Phys.Rev.Lett. **108**, 081807 (2012), 1108.0695
- [16] A. Ali, P. Ball, L. Handoko, G. Hiller, Phys.Rev. **D61**, 074024 (2000), hep-ph/9910221
- [17] C. Bobeth, G. Hiller, G. Piranishvili, JHEP **12**, 040 (2007), 0709.4174
- [18] R. Aaij et al. (LHCb Collaboration) (2012), 1209.4284
- [19] F. Mahmoudi, S. Neshatpour, J. Orloff, JHEP **08**, 092 (2012), 1205.1845
- [20] W. Altmannshofer, D.M. Straub, JHEP **08**, 121 (2012), 1206.0273